The nonhydrostatic ICON model: Transport on icosahedral-triangular grids

Daniel Reinert
German Weather Service (DWD)
(daniel.reinert@dwd.de)

1 Introduction

The joint project ICON (**ICO**sahedral **N**onhydrostatic model) initiated by the Max Planck Institute for Meteorology (MPI-M) and the German Weather Service (DWD) aims at developing a new coupled atmosphere-ocean modeling system for global numerical weather prediction (NWP) and climate research.

The horizontal grid is constructed from an icosahedron inscribed inside the unit sphere which provides a quasi-uniform coverage of the sphere, thus solving the pole problem. Two types of staggered C-grids are currently implemented, using either triangles or hexagons as primal grid. The triangular version allows for static local mesh-refinement, which is necessary for high resolution simulations in NWP or regional climate applications. At each refinement level, the so called parent triangles are split into 4 child triangles via bisection of the parent edges (see Fig. 1).

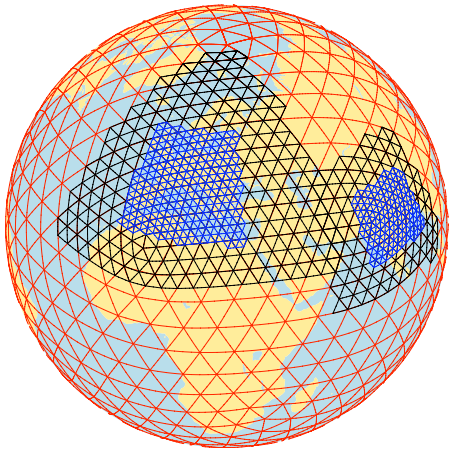

Fig. 1: *Triangular ICON-grid with two-way static mesh-refinement.*

Key aspects of the nonhydrostatic model version will be presented, putting special emphasis on our recent developments regarding transport schemes for passive tracer variables.

2 Flux-form semi-Lagrangian transport

We implemented a finite-volume flux-form semi-Lagrangian (FFSL) conservative transport scheme on the triangular mesh. It is similar to the 2D second order scheme of Miura (2007), which was originally presented for icosahedral-hexagonal meshes. Here, we pursue a higher order extension of the latter scheme on triangles.

The scheme is based on a finite-volume (or cell integrated) version of the 2D mass continuity equation and can be written as

$$\overline{\Psi}_i^{n+1} = \overline{\Psi}_i^n - \frac{1}{\Delta A_i} \sum_{e=1}^{3} s_i^e \times \iint_{a_i^e} \Psi^n(x,y)\,\mathrm{d}A\,, \quad \text{with} \quad \Psi = \rho \text{ or } \rho q. \tag{1}$$

Overbars denote control volume averages and $s_i^e = \mathrm{sgn}\,(\vec{v}\cdot\vec{n})$ indicates inflow/outflow. The surface integral on the r.h.s denotes the total (time integrated) flux of mass through edge e of the Eulerian control volume A_i. As shown in Fig. 2 for $e = 1$, this corresponds to the mass in the shaded "departure region" a_i^1 that is swept through the edge during Δt.

The overall accuracy of FFSL schemes strongly depends on two choices to be made: the approximation of the unknown scalar subgrid distribution $\Psi^n(x, y)$ and the approximation of the "departure region" a_i^e. Miura (2007) assumes rhomboidally shaped departure regions as depicted in Fig. 2. For $\Psi^n(x, y)$ he uses 2D polynomials of degree 1 (linear), and neglects that the departure region may reach beyond the Eulerian cell for which the polynomial is constructed. In order to increase the formal order of accuracy of Miura's scheme from second to third order, both the reconstruction and the approximation of the departure region would have to be improved. Improvements to the departure region, however, appear to be too costly for operational NWP applications. Therefore we investigated possible advantages of a quadratic instead of a linear least squares reconstruction for $\Psi^n(x, y)$, while retaining Miura's approximation to the departure region.

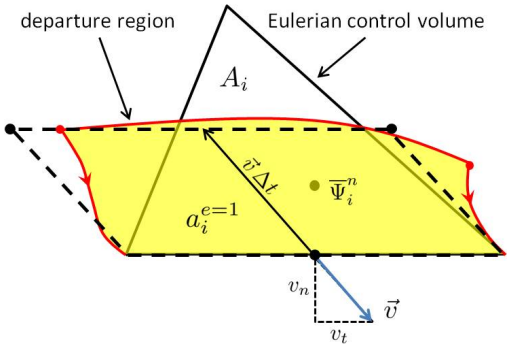

Fig. 2: *Eulerian cell A_i with departure region a_i^1 and rhomboidal approximation according to Miura (2007) (dashed).*

3 Results

Figure 3 shows results for the solid body rotation test case described in Williamson (1992), where a cosine bell is transported once around the sphere in a time independent and non-deformational flow field. It can be seen that the errors are much more symmetrically distributed when using a quadratic (b) instead of a linear (a) reconstruction. Moreover, the quadratic reconstruction shows markedly improved convergence rates (Fig. 4).

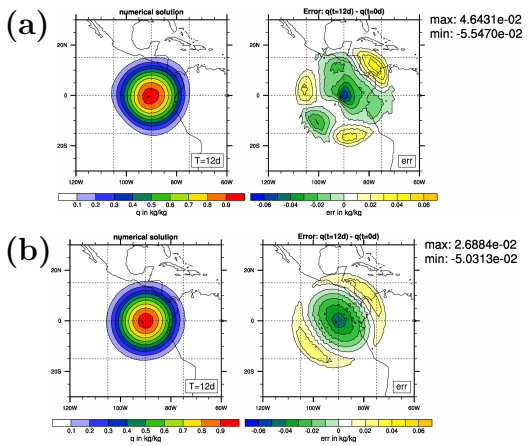

Fig. 3: *Scalar field and error after* 1 *revolution for (a) linear and (b) quadratic reconstruction.*

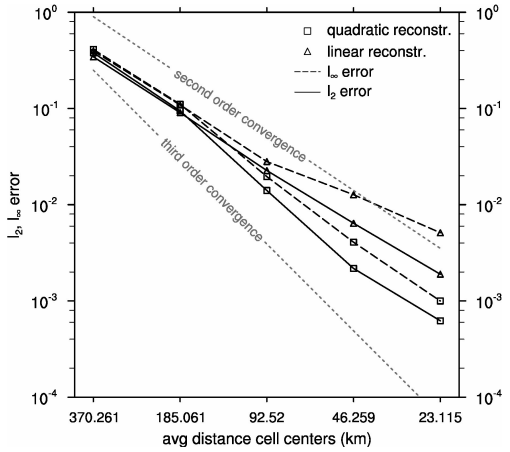

Fig. 4: *L_2 and L_∞ error norms for linear and quadratic reconstruction (*CFL ≈ 0.25*).*

A more detailed comparison in terms of local accuracy, shape-preservation, stability and computational efficiency will be presented, including results of a more challenging deformational flow test case.

Miura, H. (2007): *An upwind-based conservative advection scheme for spherical hexagonal-pentagonal grids*, Mon. Wea. Rev., **135**, 4038–4044.

Williamson, D. L. et al. (1992): *A standard test set for numerical approximations to the shallow-water equations in spherical geometry*, J. Comput. Phys., **102**, 211–224.